Published in final edited form as:
J Membr Biol. 2010 February ; 233(0): 23–33. doi:10.1007/s00232-009-9221-1.

A Single Amino Acid Change in $Ca_V1.2$ Channels Eliminates the Permeation and Gating Differences between Ca^{2+} versus Ba^{2+}

Zhe Li[1,2], **Xianming Wang**[1], **Guofeng Gao**[1], **Dongmei Qu**[1,3], **Buwei Yu**[3], **Congxin Huang**[2], **Keith S. Elmslie**[4], and **Blaise Z. Peterson**[1]

[1]Department of Cellular and Molecular Physiology, The Pennsylvania State University College of Medicine, Hershey, PA 17033, USA

[2]Department of Cardiology, Renmin Hospital and Cardiovascular Research Institute, Wuhan University, Wuhan 430060, China

[3]Department of Anesthesiology, Ruijin Hospital, Shanghai Jiao Tong University, School of Medicine, Shanghai 200025, China

[4]Departments of Anesthesiology and Pharmacology, The Pennsylvania State University College of Medicine, Hershey, PA 17033, USA

Abstract

Glutamate scanning mutagenesis was used to assess the role of the calcicludine binding segment in regulating channel permeation and gating using both Ca^{2+} and Ba^{2+} as charge carriers. As expected, wild-type L-type calcium channels had a Ba^{2+} conductance ~2× that in Ca^{2+} (G_{Ba}/G_{Ca} = 2) and activation was ~10 mV more positive in Ca^{2+} vs. Ba^{2+}. Of the eleven mutants tested, F1126E was the only one mutant that showed unique permeation and gating properties compared to wild-type. F1126E equalized the L-channel conductance (G_{Ba}/G_{Ca} = 1) and activation voltage-dependence between Ca^{2+} and Ba^{2+}. Ba^{2+} permeation was reduced because the interactions among multiple Ba^{2+} ions and the pore were specifically altered for F1126E, which resulted in Ca^{2+}-like ionic conductance and unitary current. However, high affinity block of monovalent cation flux was not altered for either Ca^{+2} or Ba^{2+}. The half activation voltage of F1126E in Ba^{2+} was depolarized to match that in Ca^{2+}, which was unchanged from wild-type. As a result, the voltages for half activation and half inactivation of F1126E in Ba^{2+} and Ca^{+2} were similar to those of wild-type in Ca^{+2}. This effect was specific to F1126E since F1126A did not affect the half activation voltage in either Ca^{+2} or Ba^{2+}. These results indicate that residues in the outer vestibule of the L-channel pore are major determinants of channel gating, selectivity and permeation.

Keywords

mutation; voltage-dependent; surface charge; outer vestibule; selectivity filter; pore; electrophysiology

INTRODUCTION

L-type calcium channels ($Ca_V1.2$) regulate Ca^{2+} influx into myocytes and neurons and are critical for regulating excitation-contraction coupling, neuronal excitability and gene expression (Catterall et al., 2005). Ion permeation and gating are two essential biophysical

Corresponding Author: Blaise Z. Peterson, Ph.D., Department of Cellular and Molecular Physiology, The Pennsylvania State University College of Medicine, 500 University Drive, P.O. Box 850, Hershey, PA 17033, USA, Tel: 717-531-8569, Fax: 717-531-0218, bpeterson@psu.edu.

properties of calcium channels and controlled by distinct channel protein domains (Hille 2001) (Fig. 1), yet both properties are considered dependent on the identity of the charge carrier. For example, ionic conductance tends to be approximately two-times larger and voltage-dependent activation and inactivation are shifted approximately 10 mV hyperpolarized when Ca^{2+} is replaced by Ba^{2+} as the charge carrier. The preference for passing Ba^{2+} ions has been explained by modeling the selectivity filter as a single-file, multi-ion pore that has a higher affinity for Ca^{2+} than for Ba^{2+} (Sather and McCleskey 2003). Stronger Ca^{2+} binding with the polar head groups of the lipid bilayer (i.e. surface charge screening) has been proposed to explain the ~10 mV positive shift in activation voltage in Ca^{2+} vs. Ba^{2+} for sodium and calcium channels (Hille 2001).

However, an increasing number of studies have found that permeation and gating are not entirely independent: for example, activation gating kinetics have been shown to influence ion selectivity of voltage-dependent potassium channels (Zheng and Sigworth 1997); the binding of alkaloid neurotoxins like veratridine and batrachotoxin to sodium channels promotes long open times and alters the selectivity properties of voltage-dependent sodium channels (Corbett and Vanderklok 1994; Naranjo and Latorre 1993); and, unlike L-type channels, ionic conductance and the voltage-dependence for activation and inactivation of T-type (Ca_V3) calcium channels are similar in Ba^{2+} and Ca^{2+} (Kaku et al. 2003; Khan et al. 2008; Klugbauer et al. 1999). The later result suggests that the screening of membrane surface charge has a smaller effect on channel gating than previously believed.

The relationship between gating and ion permeation of L-type channels has not been studied in great detail. We have previously used pharmacological agents such as dihydropyridine (DHP) antagonists and the peptide toxin calcicludine to study structural changes in the pore that are associated with the permeation and gating properties (Peterson and Catterall 2006; Wang et al. 2007). Recently, we found that calcicludine functions as a positive allosteric modulator of DHP binding and binds to three acidic residues (Glu-1122, Asp-1127 and Asp-1129) in the S5-P-helix segment in the outer vestibule of domain III (Peterson and Catterall 2006; Wang et al. 2007). These findings suggest that calcicludine can be used as a molecular tool to gain a deeper understanding of the relationship between the pore structure, permeation and channel gating.

Since calcicludine is a highly basic peptide consisting of 13 positively charged lysine or arginine residues and only 2 negatively charged glutamate residues, we used glutamate-scanning mutagenesis of the calcicludine binding region (Fig. 1) to determine whether the introduction of additional negative amino acids would affect L-channel calcicludine binding. Unfortunately, none of the mutant channels exhibited an affinity for calcicludine significantly higher than that of wild-type L-channels. However, in the process of characterizing the functional properties of the mutant channels, we found that the permeation and gating properties of F1126E measured in Ba^{2+} became "Ca^{2+}-like". The conductance, half-activation voltage and half-inactivation voltage of the mutant F1126E measured in Ba^{2+} and Ca^{2+} were the same and resembled those of the wild-type L-channel in Ca^{2+}. These findings are consistent with previous reports suggesting that differences in the effects of divalent cation screening on channel gating are located in or near the pore (Kass and Krafte 1987; Wilson et al. 1983; Zamponi and Snutch 1996). Our results further suggest that common structural elements within the outer vestibule of the pore modulate both permeation and gating of L-type calcium channels.

MATERIALS AND METHODS

Glutamate-scanning mutagenesis

Site-directed mutagenesis was used to sequentially replace 13 amino acid residues in the calcicludine binding segment (Trp-1121 to Met-1136) with glutamate. Mutant fragments of the channel were generated by polymerase chain reaction (PCR) using mutagenic primers designed to overlap with an engineered NheI site at positions 1131/1132 in the P-loop of repeat III of the L-type calcium channels (Wei et al. 1991). The mutant PCR products were gel purified, digested using EcoRI/NheI (W1121E through V1131E) or NheI/BseEII (L1132E through M1136E) restriction endonucleases and subcloned into EcoRI/NheI- or NheI/BstEII- digested $Ca_V1.2$ vector. The presence of the mutation and the integrity of each mutant were confirmed by qualitative restriction map analysis and directional DNA sequence analysis of the entire subcloned region. Functional expression of the mutant cDNAs was confirmed by Western blot analysis and whole-cell patch-clamp electrophysiology.

Cell culture and transfections

HEK293 cells were grown at 37°C and 6% CO_2 in DMEM-F12 medium supplemented with 10% fetal bovine serum and 1% Penn Strep antibiotics. cDNAs encoding wild-type and mutant $Ca_V1.2$ channels were cotransfected with $\alpha_2\delta$ (Tomlinson et al. 1993), β_{2a} (Perez-Reyes et al. 1992) and CaM_{1234} (Peterson et al. 1999) into HEK293 cells by calcium phosphate precipitation as described previously (Peterson et al. 1999; Wang et al. 2005). CaM_{1234} was used to eliminate complications that could arise from Ca^{2+}/CaM-dependent changes in channel gating, since it encodes an inactive form of calmodulin that has been shown to eliminate Ca^{2+}-dependent inactivation and facilitation (Peterson et al. 1999; Peterson et al. 2000; Qin et al. 1999; Wang et al. 2005; Zuhlke et al. 1999). All cDNAs were expressed using pcDNA3 mammalian expression plasmids (Invitrogen, Carlsbad, CA).

Patch-clamp electrophysiology

Whole-cell patch-clamp recordings were acquired as described previously (Wang et al. 2005). Briefly, whole-cell currents were recorded at room temperature 2–3 days after transfection. Pipettes were pulled from borosilicate glass using a P-97 Flaming/Brown micropipette puller (Sutter Instruments, Novato, CA) and fire polished on a MF200 microforge (World Precision Instruments, Sarasota, FL). Four types of external solutions are used for whole-cell recordings: 1) external solutions containing 30 mM Ba^{2+} or Ca^{2+} were used in the initial screen of all the mutant channels to increase the probability that currents could be recorded from poorly-expressing mutant channels (in mM): N-methyl-D-glutamine (NMG)-aspartate, 130; HEPES, 10; 4-aminopyridine, 10; and $BaCl_2$ or $CaCl_2$, 30. The osmolarity was adjusted to 300 mmol/kg with glucose and the pH was adjusted to 7.4 using 1 mM NMG base solution; 2) Concentrations of $BaCl_2$ and $CaCl_2$ were reduced to 10 mM to assure proper voltage clamp of currents used in more detailed studies described in Figs. 3, 4 and 5D-F; 3) Bath solutions used to measure Ba^{2+}- or Ca^{2+}- dependent block of Li^+ currents (Fig. 7) contained (in mM): LiCl, 100; HEPES, 10; TEA-Cl, 14; EDTA, 5; HE-EDTA, 5; and $BaCl_2$ or $CaCl_2$, as needed based on published binding constants (WINMAXC, Chris Patton, Stanford University). The indicated concentrations of free divalent cations were [Ba^{2+}] (in μM) 0.3, 1, 3, 10, 30, 100 and [Ca^{2+}] (in nM) 10, 30, 100, 300, 1000, 10000. pH was adjusted using TEA-OH, and the osmolarity was adjusted to 300 mmol/kg using TEA-Cl; 4) External solutions similar to those used in No. 1 were used in experiments that assess current-concentration relationships (Fig. 8), except that the concentrations of $BaCl_2$ or $CaCl_2$ were 3, 10, 30 and 100 mM and glucose and NMG were added or removed as necessary to maintain the desired osmolarity of 300 mmol/kg. 5) The 10 mM Ba^{2+} external solution described under No. 2 was used in experiments to determine the response of each

mutant channel to calcicludine. Each mutant was tested using calcicludine concentrations of 50 (<10% wild-type block) and 500 (~ wild-type IC_{50}) nM. The internal solution for all experiments contained (in mM): NMG-$MeSO_3$, 140; EGTA, 10; $MgCl_2$, 1; Mg-ATP, 4; and HEPES, 10. The osmolarity was adjusted to 300 mmol/kg with glucose and the pH was adjusted to 7.4 with NMG base. Pipettes had resistances of 2.5–3.0 MΩ when filled with internal solution.

Data acquisition and analysis

Data were acquired using a HEKA EPC-9/2 amplifier and PULSE/PULSEFIT software (HEKA Electronic, Lambrecht, Germany). Leak and capacitive transients were corrected by −P/4 compensation. Series resistance was <6 MΩ and compensated to 70%. Tail currents and data acquired for nonstationary noise analysis were sampled at 50 kHz, and filtered at 5.0 kHz and 10 kHz, respectively. All the other currents were sampled at 20 kHz, and filtered at 3.0 kHz. Pulse protocols are described in each figure legend.

Data analysis was performed using FITMASTER and PULSETOOLS (HEKA Electronic, Lambrecht, Germany) and Origin 7 (Originlab, Northampton, MA). Nonstationary noise analysis (Sigworth 1977; Sigworth 1980) was performed to obtain information on single-channel parameters such as the unitary current amplitude (i), maximal open-probability (P_o) and number of active channels (N). A series of 100 × 15 msec depolarization steps were evoked from a holding potential of −120 mV to 0 mV for both wild-type and F1126E channels with Ca^{2+} or Ba^{2+} as the charge carrier. The ensemble variance (σ^2) plotted against the mean current (I) was fitted with the parabolic function:

$$\sigma^2 = i \times I - I^2/N - \sigma_b^2$$

where σ_b^2 is the baseline variance.

All data are reported as means ± SEM. Statistically significant results ($p < 0.05$) are indicated in the figures by an asterisk (*) for comparisons between wild-type and mutant channels and a pound sign (#) when comparing a particular channel variant (wild-type or mutant) in Ca^{2+} vs. Ba^{2+}.

RESULTS

F1126E conducts Ba^{2+} ions as if they were Ca^{2+}

An alignment of the calcicludine binding segment in domain III of $Ca_V1.2$ with the corresponding segments from other members of the high voltage-gated calcium channel family indicates that this segment is highly conserved (Fig. 1B). Each $Ca_V1.2$ residue depicted in Fig. 1B was replaced with glutamate and, of the 13 positions investigated (1121–1136) in this study, only F1128E and A1134E failed to produce measurable currents. As previously observed (Wang et al. 2005), switching from Ba^{2+} to Ca^{2+} produces a two-fold decrease in wild-type currents at all potentials between −30 to +30 mV (Fig. 2A). Of the all the mutant channels screened, only F1126E yielded an $I_{Ba(max)}/I_{Ca(max)}$ that differed from wild-type (Figs. 2B–C). In fact, Ca^{2+} currents through F1126E tended to be larger than Ba^{2+} currents (Fig. 2B).

The normalization of Ca^{2+} and Ba^{2+} currents by F1126E could be explained if Ca^{2+} permeation became more Ba^{2+}-like or vise versa. This was assessed by measuring instantaneous current-voltage relationships from tail currents from which we determined whole-cell conductance (Fig. 3) and nonstationary noise analysis from which we estimated single channel properties (Fig. 4). As expected, the normalized maximum slope conductance (G) for wild-type is approximately two-fold larger in Ba^{2+} vs. Ca^{2+} (Figs. 3C and E). In contrast, G_{Ba} is dramatically reduced for F1126E while G_{Ca} for F1126E and wild-type do

not differ (Figs. 3C–D). The summarized data in Fig. 3E indicate that Ba^{2+} conductance for F1126E is reduced such that it is indistinguishable from Ca^{2+} conductance for wild-type or F1126E.

The above results support a decreased unitary current for F1126E in Ba^{2+}, but other possibilities such as decreased P_O and/or the number of active channels cannot be excluded. As shown previously (Bean 1985), nonstationary noise analysis is well suited for estimating single channel properties from whole-cell voltage-clamp recordings because of the low background noise associated with this technique. Therefore, we used nonstationary noise analysis to obtain unitary current amplitude (*i*) for wild-type and F1126E currents in both Ca^{+2} and Ba^{2+} (Fig. 4). Mean current and variance were determined as described in the Materials and Methods. For wild-type, *i* was approximately two-fold larger in Ba^{2+} vs. Ca^{2+}. In contrast, i_{Ba} was selectively reduced for F1126E, since i_{Ca} was not significantly different from wild-type (Fig. 4E). Thus, the data in Figs. 3 and 4 indicate that the F1126E mutation selectively alters Ba^{2+} conductance so that it becomes indistinguishable from that in Ca^{2+}.

Substitution of glutamate for Phe-1126 alters the gating properties of Ca_V 1.2 channels

The voltage-dependence of activation for wild-type is ion dependent, such that peak current measured in Ca^{2+} occurs approximately 10 mV more positive than in Ba^{2+} (Fig. 2A). In contrast, switching from Ba^{2+} to Ca^{2+} failed to shift the *I–V* for F1126E channels (Fig. 2B) so that voltage-dependent activation in Ba^{2+} resembled that in Ca^{2+} (*dashed lines*). The effect of replacing Phe-1126 with glutamate on the voltage-dependence of activation was assessed in greater detail by measuring tail current amplitudes following a series of depolarizing steps ranging from −90 to +80 mV (Figs. 5A–C). As expected, half-activation voltage (V_h) was right-shifted in Ca^{2+} vs. Ba^{2+} for wild-type L-channels. In contrast, no difference in V_h was observed in Ca^{2+} vs. Ba^{2+} for F1126E. Summarized data in Fig. 5C for F1126E indicate that V_h values determined in Ca^{2+} and Ba^{2+} were indistinguishable, and were not significantly different from V_h determined for wild-type measured in Ca^{2+}. Only one other mutant (L1132E) showed a statistically similar V_h in Ba^{2+} and Ca^{+2}, but, unlike F1126E, the V_h values in neither Ba^{2+} or Ca^{+2} differed from those for wild-type L-channels (Fig. 5C). Thus, the F1126E mutation alters the channel so that the activation gating mechanism no longer distinguishes Ba^{2+} from Ca^{2+}.

V_h for steady-state inactivation of L-type calcium channels is typically 10 mV left-shifted in Ba^{2+} compared to Ca^{2+} (Hille 2001). Thus, we wanted to determine whether steady-state inactivation of F1126E in Ba^{2+} and Ca^{2+} differ from that of wild-type (Figs. 5D–F). As expected, V_h for steady-state inactivation was left-shifted in Ba^{2+} vs. Ca^{2+} for wild-type. However, no ion-dependent difference in V_h was observed for F1126E. In addition, V_h values for F1126E in Ba^{2+} and Ca^{2+} are not different from V_h determined for wild-type in Ca^{2+} (Fig. 5F). Thus, as was observed for permeation and activation, the voltage-dependent inactivation gating mechanism of F1126E responds to Ba^{2+} as if it were Ca^{2+}.

The gating shift in wild-type channels induced by switching from Ca^{2+} to Ba^{2+} appears to be reflected in the kinetics of channel closing (deactivation), as well. To investigate this more closely, tail currents at voltages ranging from 0 to −80 mV (following a 50 ms +50 mV step) were fit using a single exponential equation to yield the time constant (τ) of deactivation. Figure 6 shows that deactivation of wild-type channels in Ca^{2+} tended to be faster than that in Ba^{2+}, but this difference was not statistically significant at any voltage. Furthermore, τ measured from F1126E channels were not different in Ca^{2+} versus Ba^{2+}, and closely match the values measured from wild-type channel measured in Ca^{2+}. The small differences in deactivation are in the direction expected from changes in activation V_h.

Phe-1126 does not form part of a Ca^{2+} binding site in the outer vestibule of the pore

One possible explanation of our results is that Phe-1126 forms part of a cation binding site capable of distinguishing between Ca^{2+} and Ba^{2+}, and the glutamate substitution could expand that site to permit Ba^{2+} binding. We constructed the mutant F1126A, which is predicted to disrupt Ca^{2+} binding to this site. If Phe-1126 contributes to a Ca^{2+}-selective binding site, the voltage-dependence for activation in Ca^{2+} should shift in the hyperpolarizing direction such that it coincides with that determined for wild-type channels in Ba^{2+}. In other words, activation V_h for F1126A measured in Ca^{2+} should become Ba^{2+}-like. Results from these studies (Fig. 7) demonstrate that V_h for activation measured in Ca^{2+} for F1126A does not differ from wild-type and F1126E, indicating that alanine substitution at 1126 does not disrupt Ca^{2+} binding to this putative site.

F1126E alters low but not high affinity cation binding to the selectivity filter

Another possibility is that the introduction of a negative charge at position 1126 selectively alters pore configuration to normalize the binding of Ba^{2+} or Ca^{2+} within the selectivity filter, which shows higher affinity for Ca^{2+} relative to Ba^{2+} for wild-type calcium channels (Kostyuk et al. 1983). We compared the properties of high and low affinity divalent cation binding to the pore for wild-type vs. F1126E channels. The IC_{50} for half-maximal block of Li^+ currents by Ca^{2+} (Fig. 8, open symbols) and Ba^{2+} (solid symbols) was used to estimate the dissociation constants for the high affinity binding of Ca^{2+} and Ba^{2+} ions to the selectivity filter. Substituting Phe-1126 with glutamate does not alter the IC_{50} values for block of Li^+ currents by either Ca^{2+} or Ba^{2+} (Fig. 8). These findings indicate that the decreases in Ba^{2+} conductance exhibited by F1126E do not result from changes in the interactions of individual Ba^{2+} ions in the pore.

We next wanted to determine whether replacing Phe-1126 with glutamate alters the interactions of multiple divalent cations in the pore of the mutant channel. To test this, we compared peak tail currents generated in bath solutions containing 3, 10, 30 and 100 mM Ba^{2+} or Ca^{2+} in the same cell (Fig. 9). In Fig. 9A–B, tail currents were measured from wild-type or F1126E channels at the indicated Ba^{2+} and Ca^{2+} concentrations and the resulting current-concentration relationship was fit using the Michaelis-Menton equation. Fig. 9B shows that normalized F1126E currents in Ba^{2+} overlapped those in Ca^{2+}, resulting in a ~3-fold decrease in K_S for F1126E in Ba^{2+} compared to wild-type. Consequently, K_S for F1126E in Ba^{2+} did not differ from that determined for Ca^{2+} in either wild-type or F1126E channels (Fig. 9B and C). These results indicate that the identity of the residue at position 1126 determines the magnitude of G_{Ba}/G_{Ca} by specifically altering how multiple Ba^{2+} ions interact in the pore.

DISCUSSION

We used glutamate-scanning mutagenesis in the S5/P-helix segment of repeat III to assess the role of amino acids within the calcicludine binding segment in determining the permeation and gating characteristics of the $Ca_V1.2$ channel. Of all the glutamate substitutions screened in this study, F1126E was unique in that permeation and gating in Ba^{2+} became Ca^{2+}-like, while neither of these parameters were altered when Ca^{2+} was the charge carrier. Ba^{2+} conductance was decreased approximately two-fold and the voltage-dependence of activation and inactivation was depolarized to match that measured in Ca^{2+}.

Replacement of Phe-1126 with glutamate alters $Ca_V1.2$ channel permeation

Amino acid substitutions within the highly conserved (EEEE) selectivity filter alter ion selectivity and permeation of $Ca_V1.2$ channels (Sather and McCleskey 2003). Others (Dilmac et al. 2003; Dilmac et al. 2004; Williamson and Sather 1999) and we (Wang et al.

2005) have studied the influence on permeation of amino acids proximal to the pore glutamates of $Ca_V1.2$ channels. In the rat L-channel, mutation of the threonine near the pore glutamate to alanine in domains II and III results in a loss of selectivity between Ba^{2+} and Ca^{2+} (Dilmac et al. 2003; Dilmac et al. 2004). Similar results have been observed for domain III phenylalanine to glycine mutation in both the rat (F1117G) and rabbit (F1144G) L-type calcium channels (Dilmac et al. 2003; Dilmac et al. 2004; Wang et al. 2005). These mutations appear to disrupt Ca^{2+} affinity suggesting that the selectivity filter configuration is affected. However, our finding that the F1126E mutation failed to alter half-maximal block of Li^+ currents by either Ca^{2+} or Ba^{2+} suggests that the selectivity filter is not altered when single divalent cations compete with Li^+ for occupancy of the pore. In our results, divalent ion permeation is affected so that apparent Ba^{2+} affinity for the low affinity permeation site(s) within the pore is increased by F1126E to match the apparently unchanged affinity of the channel for Ca^{2+}. These later findings suggest that the interactions of multiple divalent cations in the pore of the channel are altered by F1126E.

These findings resemble those of Wang et al., who also found that unitary Ba^{2+} conductance for F1144G decreases to match that of Ca^{2+} (Wang et al. 2005). In this work, the "volume exclusion/charge neutralization" model was used to explain the reduced conductance of Ba^{2+} but not Ca^{2+} through the pores of the $Ca_V1.2$ mutant channels F1144G, Y1152K, and FY/GK (Peterson and Catterall 2006; Wang et al. 2005). The crystal diameters of Ca^{2+} and Na^+ ions are nearly identical (2.00 versus 2.04 Å, respectively), yet each Ca^{2+} ion carries twice as much countercharge as a Na^+ ion. Therefore, Ca^{2+} binds tightly to the selectivity filter because it is able to neutralize the highly charged EEEE locus without the over crowding suspected for monovalent cations (i.e. too many ions in the pore attempting to neutralize the negative charges). Ba^{2+} and Ca^{2+} ions carry the same charge, but the ionic diameter of Ba^{2+} is approximately 36% larger than that of Ca^{2+}. Thus, for wild-type channels, Ba^{2+} ions are expected to exhibit a higher degree of crowding as multiple ions attempt to bind/neutralize the EEEE negative charges, which is thought to explain the lower binding affinity and consequentially increasing the exit rate (i.e., larger conductance) relative to Ca^{2+}. Likewise, this model suggests that Ba^{2+} conductance is reduced for F1126E because Ba^{2+} ions in this pore are less prone to over crowding. However, it is not clear how a change within the pore that would increase the apparent Ba^{2+} affinity would not impact Ca^{+2}.

Replacement of Phe-1126 with glutamate alters $Ca_V1.2$ channel gating

The mechanism by which Ca^{2+} or Ba^{2+} affects activation gating could result from effects on either closed-closed gating transitions (Yarotskyy et al. 2009) or on closed-open transitions (Marks and Jones 1992). We reasoned that the gating effect of the F1126E mutation could be localized to either closed-closed or closed-open transitions by investigating the impact on closed-state inactivation. We found that the effect of the mutation on the closed-state inactivation V_h was similar to that measured from activation, which supports the idea that the mutation affects closed-closed transitions. Transitions between $Ca_V1.2$ channel closed state are voltage dependent, while the closed-open transitions are voltage-independent (Marks and Jones 1992). Thus, Ca^{2+} and Ba^{2+} appear to affect voltage sensor movement (i.e. the S4 segment). One scenario is that divalent cation binding electrostatically impedes voltage sensor movement. However, we cannot rule out other mechanisms such as allosterically-induced conformational changes that impact channel activation.

Surface charge screening is the classical explanation for the effect of Ca^{2+} and Ba^{2+} on the gating of voltage-dependent channels gating. The idea is that local negative electric fields are set up by phosphate head groups at the lipid membrane surface, and these charges bias the transmembrane voltage sensed by the channel voltage sensors (Hille 2001). Stronger Ca^{2+} binding with the interface negative charges was the explanation for the ~10 mV

positive voltage shift observed with equimolar exchange of Ca^{2+} for Ba^{2+} for both sodium channels (Hanck and Sheets 1992; Hille et al. 1975; Ohmori and Yoshii 1977) and calcium channels (Byerly et al. 1985; Cota and Stefani 1984; Ganitkevich et al. 1988; Kass and Krafte 1987; Ohmori and Yoshii 1977; Smith et al. 1993; Wilson et al. 1983; Zamponi and Snutch 1996). However, this idea was recently challenged when it was found that T-type calcium channels fail to show such a voltage shift (Kaku et al. 2003; Khan et al. 2008; Klugbauer et al. 1999), which implied that the surface charge is specific to a particular ion channel. Our findings further support this idea by showing that the F1126E point mutation nullifies the L-type calcium channel gating difference between Ca^{2+} and Ba^{2+}. We previously identified a set of pore mutations that abrogated Ca^{2+}-Ba^{2+} gating shift, F1144G/Y1152K (Wang et al. 2005). Neither F1144G nor Y1152K significantly affect L-type calcium channel gating in either Ca^{2+} or Ba^{2+}, but with both mutations together Ca^{2+} no longer right-shifted V_h. However, this change is opposite of what we have observed with F1126E, since V_h is significantly right-shifted by this mutation to equal that in Ca^{2+} for both wild-type and F1126E L-type calcium channels. The F1144G/Y1152K double mutant reduces Ba^{2+} conductance to that of Ca^{2+}, so that effect on permeation (Ba^{2+} to Ca^{2+}) is opposite that for gating (Ca^{2+} to Ba^{2+}) (Wang et al. 2005). In the case of F1126E, the effect on permeation and gating are convergent in that the channel responds to Ba^{2+} as if it were Ca^{2+}.

This convergence suggests that Ca^{2+} binds to a site on Ca_V channels to affect both gating and permeation, but this site has little or no affinity for Ba^{2+}. The F1126E mutation alters the Ca^{2+} binding site so that it can accommodate Ba^{2+} as effectively as it does Ca^{2+}. Two possibilities are that the location of such a site could be the selectivity filter or formed amino acids in the outer vestibule of the pore. In support of the selectivity filter hypothesis, permeation models such as the size exclusion model discussed above provide a quantitative basis on which to understand that apparent increased affinity of the pore for Ba^{2+}. However, it is currently believed that Ba^{2+} binds within the pore of wild-type channels (albeit with lower affinity), which creates a problem for explaining the voltage dependent shift in gating in Ca^{2+} vs. Ba^{2+}. In support of the second possibility, previous reports have suggested that differences in the effects of divalent cation surface charge screening on channel gating are dependent on a selective Ca^{2+} binding site in the outer vestibule of the channel pore (Kass and Krafte 1987; Wilson et al. 1983; Zamponi and Snutch 1996). However, our attempt to disrupt Ca^{2+} binding to this putative site was unsuccessful since the F1126A mutation failed to alter the response of the channel to Ca^{2+} (or Ba^{2+}). A scenario that is consistent with all of our results is that amino acids within the outer vestibule form a binding site that is selective for Ca^{2+}, but Phe-1126 is not involved in forming this binding site. However, the Phe-Glu substitution at position 1126 modifies that site enabling it to accommodate the larger Ba^{2+} ions while not altering the affinity of the site for Ca^{2+}. Thus, the binding of both Ca^{2+} and Ba^{2+} to this site results in low conductance for both ions through the pore and a depolarizing shift in channel gating. Additional outer pore mutations within each $Ca_V1.2$ channel domain will be required to more completely understand the underlying mechanism by which F1126E affects Ba^{2+}-channel interaction.

Regardless of the precise mechanism, our results provide further support for an interaction between ion occupancy of the pore and calcium channel gating (Babich et al. 2007; Cens et al. 2007; Li et al. 2004; Li et al. 2005; Wang et al. 2005). More specifically we have identified a single amino acid responsible for setting the differential gating and permeation response of the L-type calcium channel to Ca^{2+} vs. Ba^{2+}. The mutation of this site from phenylalanine to glutamate appears to slow Ba^{2+} flux through the pore so that it equals that of Ca^{2+}. Furthermore, this mutation specifically shifts channel activation to more depolarized voltages so that V_h equals that in Ca^{2+}, which was not affected by the mutation.

The fact that mutation of amino acids on either side of Phe-1126 failed to significantly affect either permeation or gating further demonstrates the specificity of this site.

Acknowledgments

We thank Yunhua Wang for great technical assistance.

GRANT SUPPORT

This project is funded in part by grants from the Pennsylvania Department of Health using Tobacco Settlement Funds and the National Institutes of Health HL074143 (B.Z.P.) and the China Scholarship Council, Chinese Scholarship Fund (Zhe Li).

REFERENCES

Babich O, Matveev V, Harris AL, et al. Ca^{2+}-dependent inactivation of Ca(V)1.2 channels prevents Gd^{3+} block: Does Ca^{2+} block the pore of inactivated channels? J Gen Physiol. 2007; 129:477–483. [PubMed: 17535960]

Bean BP. Two kinds of calcium channels in canine atrial cells. Differences in kinetics, selectivity and pharmacology. J Gen Physiol. 1985; 86:1–30. [PubMed: 2411846]

Byerly L, Chase PB, Stimers JR. Permeation and interaction of divalent cations in calcium channels of snail neurons. J Gen Physiol. 1985; 85:491–518. [PubMed: 2409216]

Catterall WA, Perez-Reyes E, Snutch TP, Striessnig J. International Union of Pharmacology. XLVIII. Nomenclature and structure-function relationships of voltage-gated calcium channels. Pharmacol Rev. 2005; 57:411–425. [PubMed: 16382099]

Cens T, Rousset M, Kajava A, et al. Molecular determinant for specific Ca/Ba selectivity profiles of low and high threshold Ca^{2+} channels. J Gen Physiol. 2007; 130:415–425. [PubMed: 17893194]

Corbett AM, Vanderklok MA. Sodium-channel subtypes in the rat display functional differences in the presence of veratridine. Biochem Biophys Res Commun. 1994; 199:1305–1312. [PubMed: 8147874]

Cota G, Stefani E. Saturation of calcium channels and surface charge effects in skeletal muscle fibres of the frog. J Physiol. 1984; 351:135–154. [PubMed: 6086902]

Dilmac N, Hilliard N, Hockerman GH. Molecular determinants of Ca^{2+} potentiation of diltiazem block and Ca^{2+}-dependent inactivation in the pore region of Ca(v)1.2. Mol Pharmacol. 2003; 64:491–501. [PubMed: 12869655]

Dilmac N, Hilliard N, Hockerman GH. Molecular determinants of frequency dependence and Ca^{2+} potentiation of verapamil block in the pore region of Ca(v)1.2. Mol Pharmacol. 2004; 66:1236–1247. [PubMed: 15286207]

Ganitkevich V, Shuba MF, Smirnov SV. Saturation of calcium channels in single isolated smooth muscle cells of guinea-pig taenia caeci. J Physiol. 1988; 399:419–436. [PubMed: 2457091]

Hanck DA, Sheets MF. Extracellular divalent and trivalent cation effects on sodium current kinetics in single canine cardiac Purkinje cells. J Physiol. 1992; 454:267–298. [PubMed: 1335501]

Hille, B. Ion Channels of Excitable Membranes. 3rd ed.. Sunderland, MA: Sinaur Associates; 2001.

Hille B, Woodhull AM, Shapiro BI. Negative surface charge near sodium channels of nerve: divalent ions, monovalent ions, and pH. Philos Trans R Soc Lond B Biol Sci. 1975; 270:301–318. [PubMed: 238230]

Kaku T, Lee TS, Arita M, et al. The gating and conductance properties of Ca_V 3.2 low-voltage-activated T-type calcium channels. Jpn J Physiol. 2003; 53:165–172. [PubMed: 14529577]

Kass RS, Krafte DS. Negative surface charge density near heart calcium channels. Relevance to block by dihydropyridines. J Gen Physiol. 1987; 89:629–644. [PubMed: 2438373]

Khan N, Gray IP, Obejero-Paz CA, et al. Permeation and gating in Ca(V)3.1 (alpha 1G) T-type calcium channels effects of Ca^{2+}, Ba^{2+}, Mg^{2+}, and Na^{+} J Gen Physiol. 2008; 132:223–238. [PubMed: 18663131]

Klugbauer N, Marais E, Lacinova L, et al. A T-type calcium channel from mouse brain. Pflugers Arch. 1999; 437:710–715. [PubMed: 10087148]

Kostyuk PG, Mironov SL, Shuba YM. 2 selective filters in the calcium channel of the molluscan neuron somatic membrane. Neurophysiology. 1983; 15:314–319. [PubMed: 6877434]

Li JY, Stevens L, Klugbauer N, et al. Roles of molecular regions in determining differences between voltage dependence of activation of Ca(v)3.1 and Ca(v)1.2 calcium channels. J Biol Chem. 2004; 279:26858–26867. [PubMed: 15100229]

Li JY, Stevens L, Wray D. Molecular regions underlying the activation of low- and high-voltage activating calcium channels. Eur Biophys J. 2005; 34:1017–1029. [PubMed: 15924245]

Marks TN, Jones SW. Calcium currents in the A7r5 smooth muscle-derived cell line. An allosteric model for calcium channel activation and dihydropyridine agonist action. J Gen Physiol. 1992; 99:367–390. [PubMed: 1316936]

Naranjo D, Latorre R. Ion conduction in substates of the batrachotoxin-modified Na^+ channel from toad skeletal muscle. Biophys J. 1993; 64:1038–1050. [PubMed: 8388264]

Ohmori H, Yoshii M. Surface potential reflected in both gating and permeation mechanisms of sodium and calcium channels of the tunicate egg cell membrane. J Physiol. 1977; 267:429–463. [PubMed: 17734]

Perez-Reyes E, Castellano A, Kim HS, et al. Cloning and expression of a cardiac/brain beta subunit of the L-type calcium channel. J Biol Chem. 1992; 267:1792–1797. [PubMed: 1370480]

Peterson BZ, Catterall WA. Allosteric interactions required for high-affinity binding of dihydropyridine antagonists to Ca(V)1.1 Channels are modulated by calcium in the pore. Mol Pharmacol. 2006; 70:667–675. [PubMed: 16675661]

Peterson BZ, DeMaria CD, Adelman JP, et al. Calmodulin is the Ca^{2+} sensor for Ca^{2+}-dependent inactivation of L-type calcium channels. Neuron. 1999; 22:549–558. [PubMed: 10197534]

Peterson BZ, Lee JS, Mulle JG, et al. Critical determinants of Ca^{2+}-dependent inactivation within an EF-hand motif of L-type Ca^{2+} channels. Biophys J. 2000; 78:1906–1920. [PubMed: 10733970]

Qin N, Olcese R, Bransby M, et al. Ca^{2+}-induced inhibition of the cardiac Ca^{2+} channel depends on calmodulin. Proc Natl Acad Sci U S A. 1999; 96:2435–2438. [PubMed: 10051660]

Sather WA, McCleskey EW. Permeation and selectivity in calcium channels. Annu Rev Physiol. 2003; 65:133–159. [PubMed: 12471162]

Sigworth FJ. Na-current fluctuations give estimates of single-channel conductance in frog nerve. Biophys J. 1977; 17:A10–A10.

Sigworth FJ. The variance of sodium current fluctuations at the node of ranvier. J Physiol. 1980; 307:97–129. [PubMed: 6259340]

Smith PA, Aschroft FM, Fewtrell CM. Permeation and gating properties of the L-type calcium channel in mouse pancreatic beta cells. J Gen Physiol. 1993; 101:767–797. [PubMed: 7687645]

Tomlinson WJ, Stea A, Bourinet E, et al. Functional properties of a neuronal class C L-type calcium channel. Neuropharmacology. 1993; 32:1117–1126. [PubMed: 8107966]

Wang X, Du L, Peterson BZ. Calcicludine binding to the outer pore of L-type calcium channels is allosterically coupled to dihydropyridine binding. Biochemistry. 2007; 46:7590–7598. [PubMed: 17536837]

Wang X, Ponoran TA, Rasmusson RL, et al. Amino acid substitutions in the pore of the Ca(V)1.2 calcium channel reduce barium currents without affecting calcium currents. Biophys J. 2005; 89:1731–1743. [PubMed: 15980164]

Wei XY, Perez-Reyes E, Lacerda AE, et al. Heterologous regulation of the cardiac Ca^{2+} channel alpha 1 subunit by skeletal muscle beta and gamma subunits. Implications for the structure of cardiac L-type Ca^{2+} channels. J Biol Chem. 1991; 266:21943–21947. [PubMed: 1718988]

Williamson AV, Sather WA. Nonglutamate pore residues in ion selection and conduction in voltage-gated Ca^{2+} channels. Biophys J. 1999; 77:2575–2589. [PubMed: 10545358]

Wilson DL, Morimoto K, Tsuda Y, et al. Interaction between calcium ions and surface charge as it relates to calcium currents. J Membr Biol. 1983; 72:117–130. [PubMed: 6304316]

Yarotskyy V, Gao G, Peterson BZ, et al. The Timothy syndrome mutation of cardiac $Ca_V1.2$ (L-type) channels: multiple altered gating mechanisms and pharmacological restoration of inactivation. J Physiol. 2009; 587:551–565. [PubMed: 19074970]

Zamponi GW, Snutch TP. Evidence for a specific site for modulation of calcium channel activation by external calcium ions. Pflugers Arch. 1996; 431:470–472. [PubMed: 8584446]

Zheng J, Sigworth FJ. Selectivity changes during activation of mutant Shaker potassium channels. J Gen Physiol. 1997; 110:101–117. [PubMed: 9236204]

Zuhlke RD, Pitt GS, Deisseroth K, et al. Calmodulin supports both inactivation and facilitation of L-type calcium channels. Nature. 1999; 399:159–162. [PubMed: 10335846]

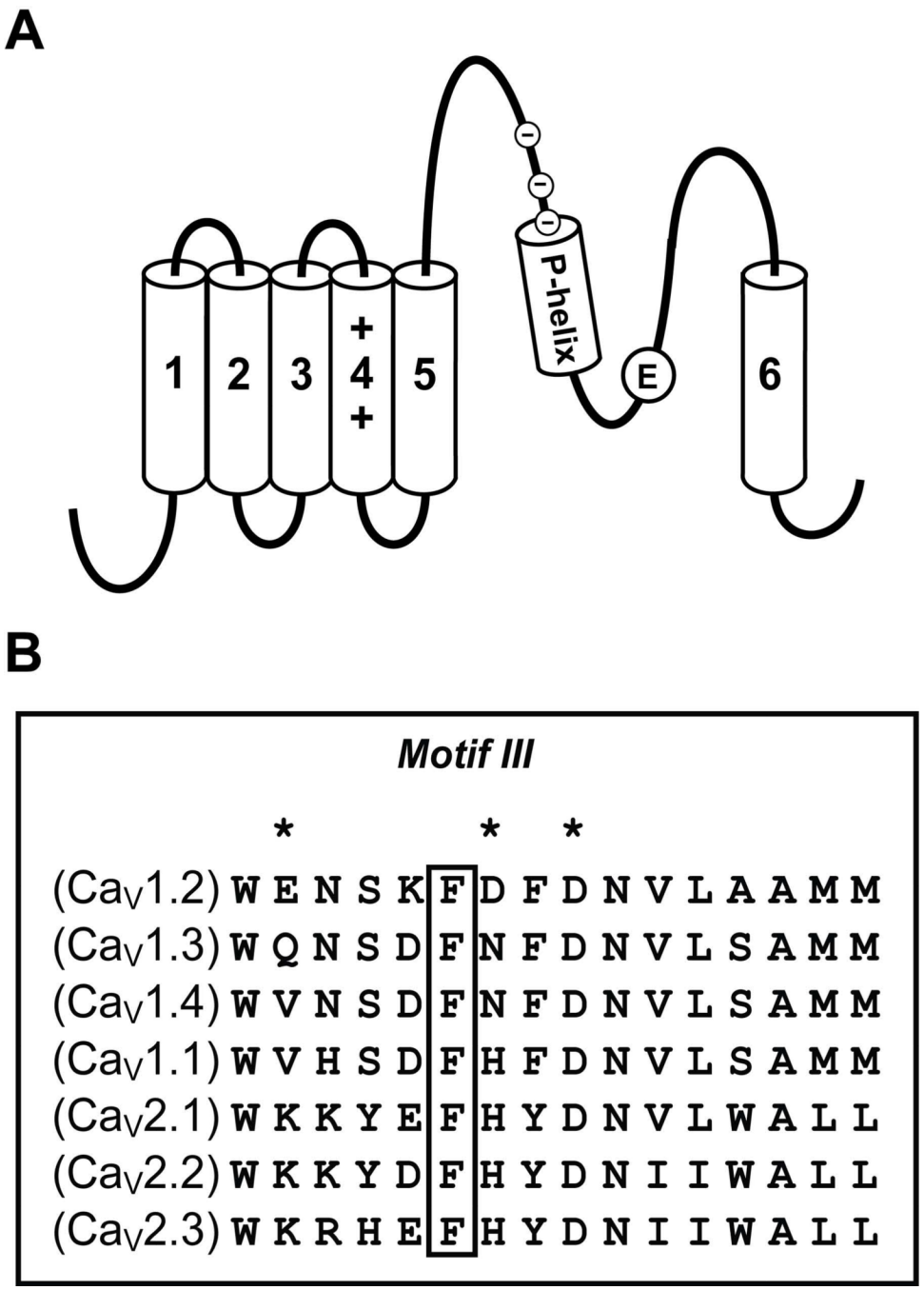

Fig. 1. The calcicludine binding region is highly conserved amongst voltage-gated calcium channel family members

(A) The membrane topology of the α1 subunit consists of four homologous repeats (repeat III is shown), each consisting of six transmembrane segments (S1–S6). The selectivity filter is formed by four conserved glutamate residues (*E*), each residing on one of the four S5–S6 connecting loops. The intracellular portions of all four S6 transmembrane segments form the inner lining of the permeation pathway and the activation gate. The S4 segment from each repeat is an amphipathic helix consisting of several positively charged lysine or arginine residues and functions as the voltage sensor that couples membrane depolarization to channel activation. Upstream of the pore-glutamate is the putative pore-helix (P-helix),

which is juxtaposed to Phe-1126 and the calcicludine binding site residues (*circled minus signs*). (B) Amino acid alignment (residues 1121 to 1136) of the calcicludine binding region. Phe-1126 is indicated with a *box* and Glu-1122, Asp-1127 and Asp-1129 are indicated with *asterisks* (*).

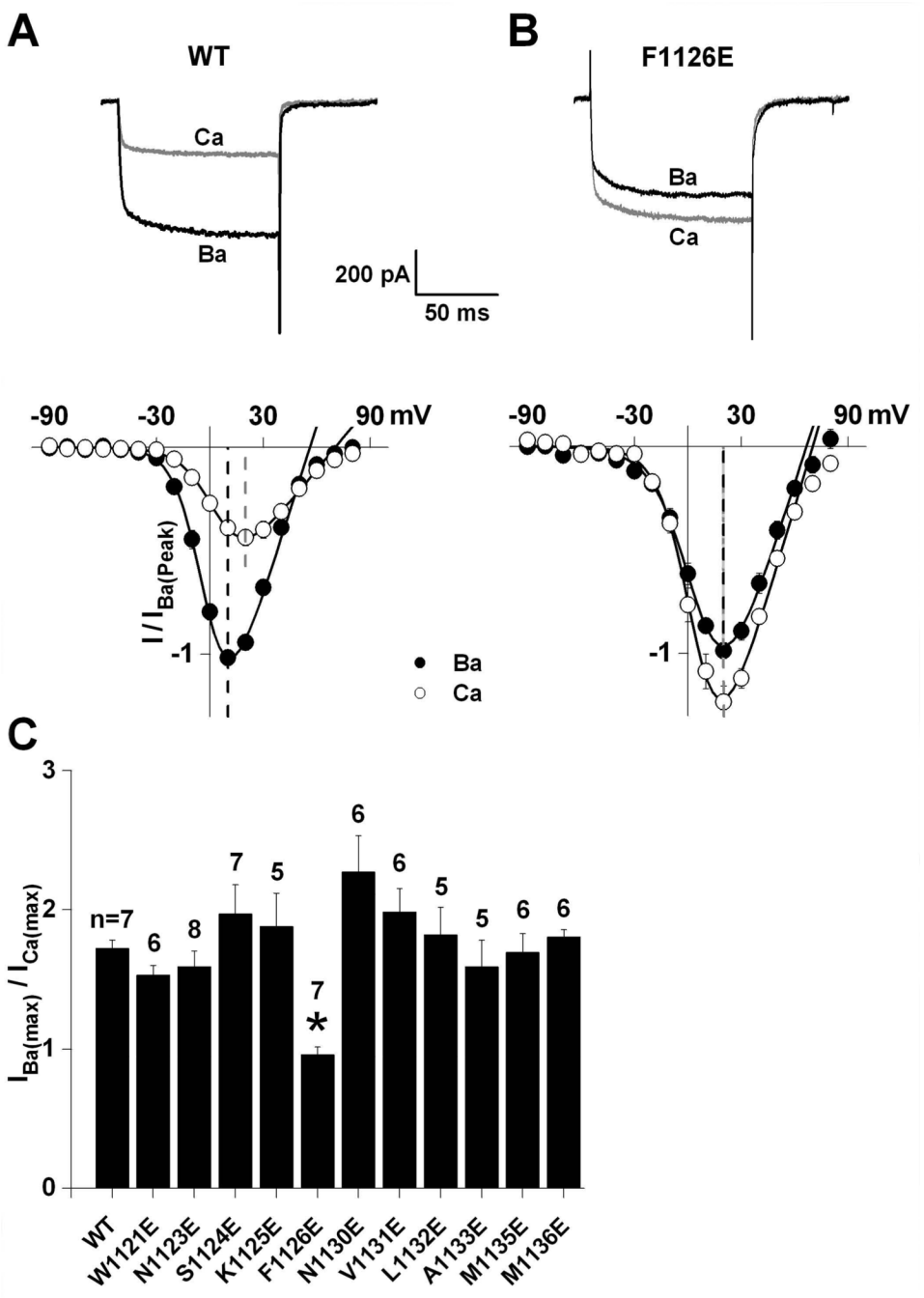

Fig. 2. Substitution of glutamate for Phe-1126 selectively alters L-channel permeation properties in Ba^{2+}

Wild-type (A) and F1126E (B) currents were evoked by 100 msec step depolarizations to +20 mV from a holding potential of −90 mV in 30 mM Ba^{2+} and Ca^{2+}. *I–V* relationships were normalized to peak Ba^{2+} currents recorded from the same cell. Dashed lines indicate peak current voltages for Ba^{2+} (black) and Ca^{2+} (gray). (C) Peak tail-currents were measured at −50 mV following 100 msec depolarizing steps ranging from −90 to +80 mV in 30 mM Ba^{2+} and Ca^{2+}. Data were fit with a Boltzmann equation through the activation vs. voltage data and normalized to maximal Ba^{2+} currents ($I_{Ba(max)}$). $I_{Ba(max)}/I_{Ca(max)}$ are

plotted for wild-type and all the mutant channels tested. Of the all the mutants investigated in this study, only F1126E was significantly different from wild-type (*).

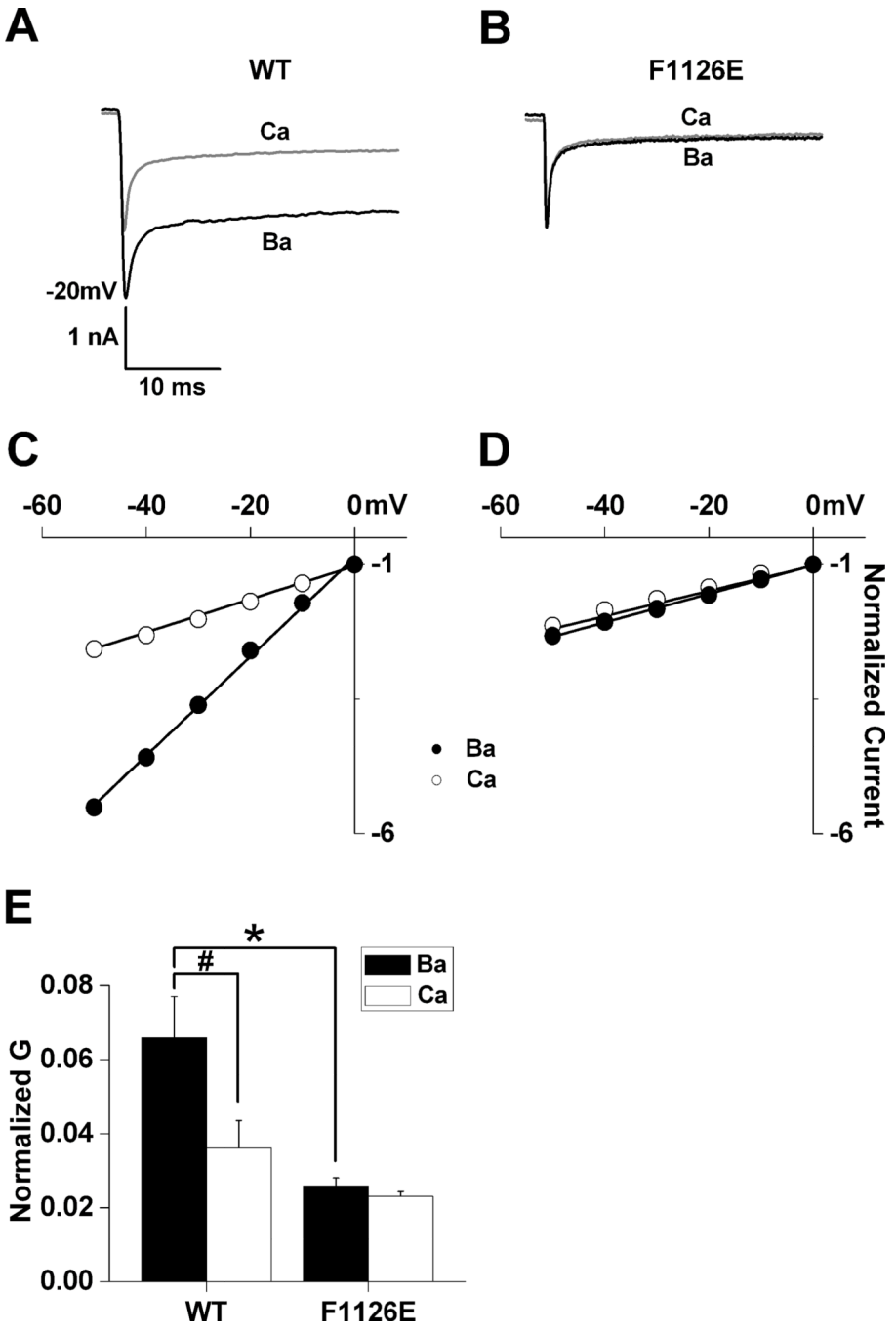

Fig. 3. F1126E conducts Ba^{2+} ions as if they were Ca^{2+}

Whole-cell conductance is a product of the single channel current amplitude, the open probability (P_o) and the number of active channels. Peak tail-currents were measured from −80 to +20 mV following 50 msec depolarizing steps to +50 mV which were used to maximally activate wild-type (A) and F1126E (B) in 10 mM Ba^{2+} and Ca^{2+} from the same cell, thus minimizing differences in P_o that could arise from shifts in the voltage-dependence of activation. Linear portions of the current-voltage relationships (−50 to 0 mV) were normalized to amplitudes measured at 0 mV for wild-type (C) and F1126E (D). Normalized data were fit with the equation $I_{tail} = G \times (V - E_{rev})$, where I_{tail} is the peak tail current, E_{rev}

the reversal potential and G the maximal slope conductance. (E) Normalized slope conductances are plotted for wild-type (n = 8) and F1126E (n = 5).

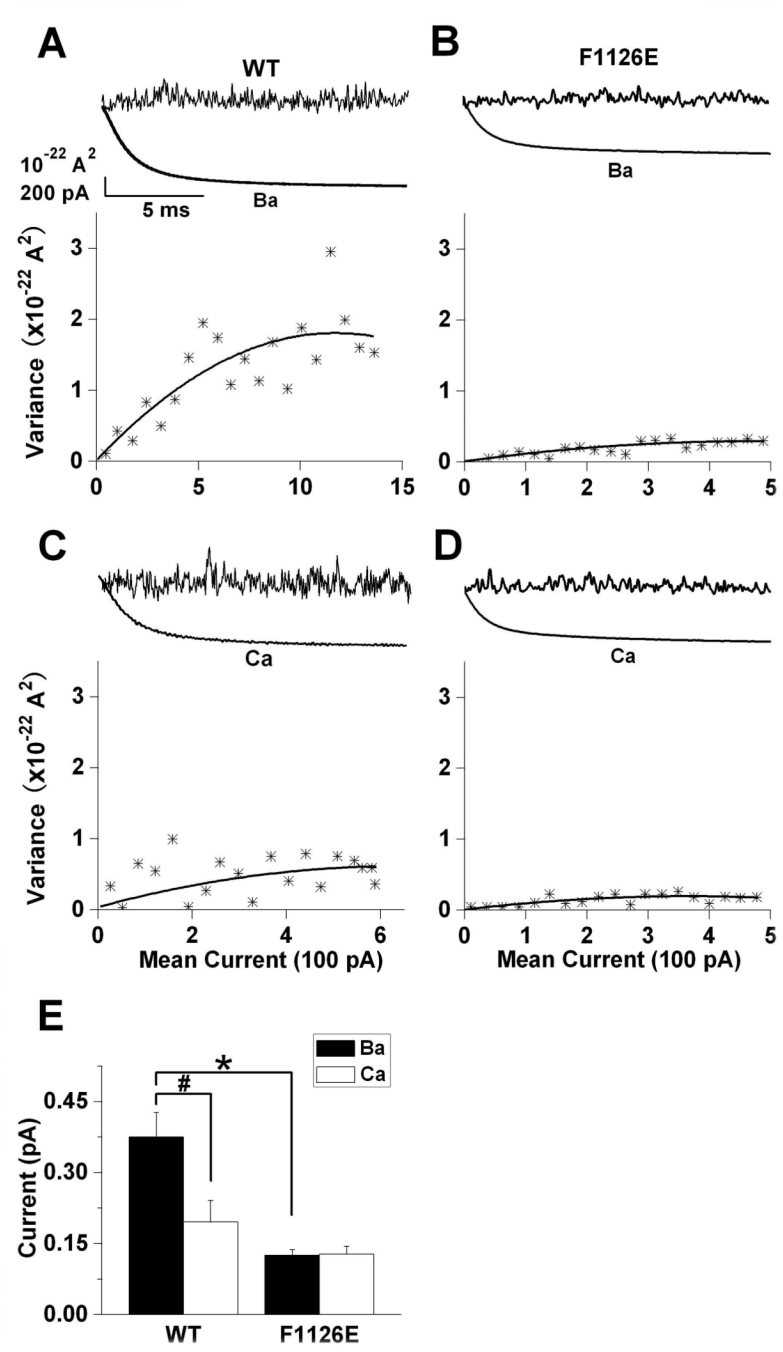

Fig. 4. F1126E reduces the unitary current amplitude in Ba^{2+} to match that in Ca^{2+}

Ba^{2+} (A and B) and Ca^{2+} (C and D) currents for wild-type and F1126E were evoked by a series of 100 voltage steps (15 msec) to 0 mV from a holding potential of −120 mV. Data were analyzed using PULSETOOLS nonstationary noise analysis software to acquire the variance and mean current of each cell (A–D, upper traces). Variance-mean current relationships (A–D, lower graphs) were fit with the equation $\sigma^2 = i \times I - I^2/N - \sigma_b^2$, where σ^2 is the variance, σ_b^2 the baseline variance or background noise, i the unitary current amplitude, I the mean current and N the number of active channels: wild-type (Ba^{2+}), i = 0.290 ± 0.019 pA, P_o = 53.8 ± 6.1%, n = 7; wild-type (Ca^{2+}), i = 0.159 ± 0.033 pA, P_o = 48.4 ± 11.6%, n = 7; F1126E (Ba^{2+}), i = 0.126 ± 0.012 pA, P_o = 42.8 ± 11.6%, n = 6;

F1126E (Ca^{2+}), i = 0.128 ± 0.017 pA, P_o = 66.9 ± 9.6%, n = 7. (E) Mean unitary current amplitudes are plotted for wild-type and F1126E.

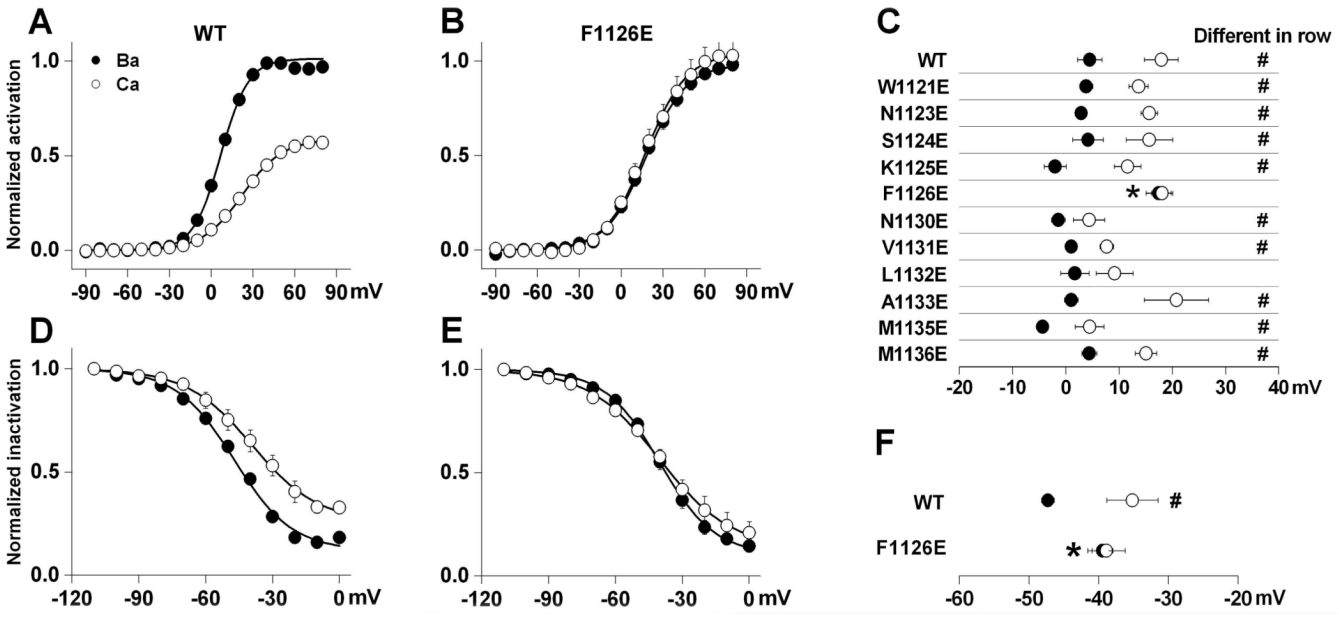

Fig. 5. Replacing Phe-1126 with glutamate selectively alters L-channel gating in Ba^{2+}

Peak tail-currents were measured at −50 mV following 100 msec depolarizing steps ranging from −90 to +80 mV in 30 mM Ba^{2+} and Ca^{2+} for wild-type (A) and F1126E (B). Tail current amplitudes recorded in Ba^{2+} and Ca^{2+} were normalized to $I_{Ba(max)}$. Boltzmann fits were used to obtain half activation voltages (V_h) and slope factors (k) (mV): wild-type (Ba^{2+}), $V_h = 4.5 \pm 2.3$, $k = 9.6 \pm 1.2$; wild-type (Ca^{2+}) $V_h = 17.9 \pm 3.2$, $k = 14.8 \pm 0.8$ (n = 7); F1126E (Ba^{2+}) $V_h = 17.4 \pm 2.4$, $k = 14.6 \pm 2.1$; F1126E (Ca^{2+}) $V_h = 18.1 \pm 2.0$, $k = 15.3 \pm 1.0$ (n = 7); (C) Mean V_h values derived from Boltzmann fits are plotted for wild-type and each mutant tested. The number of cells for each group is the same as that for Fig. 2C. (D, E) Steady-state inactivation was measured as a ratio of current elicited by 50 msec prepulses and postpulses to 0 mV (Post/Pre ratio) separated by 10 sec conditioning pulses ranging from −110 to 0 mV in 10 mM Ba^{2+} and Ca^{2+} for wild-type (D) and F1126E (E). Results from Boltzmann fits are as follows (mV): wild-type (Ba^{2+}), $V_h = -47.3 \pm 0.9$, $k = 13.1 \pm 0.2$, n = 7; wild-type (Ca^{2+}) $V_h = -35.2 \pm 3.7$, $k = 13.7 \pm 0.5$, n = 6; F1126E (Ba^{2+}) $V_h = -39.5 \pm 1.5$, $k = 12.7 \pm 1.3$, n = 6; F1126E (Ca^{2+}) $V_h = -38.9 \pm 2.7$, $k = 16.3 \pm 1.3$, n = 7. (F) Mean V_h values for steady-state inactivation are plotted for wild-type and F1126E. Significant difference in V_h between Ca^{+2} vs. Ba^{2+} (in row) is indicated by #, while * indicated significant difference between mutant and wild-type (in column) in Ba^{2+}.

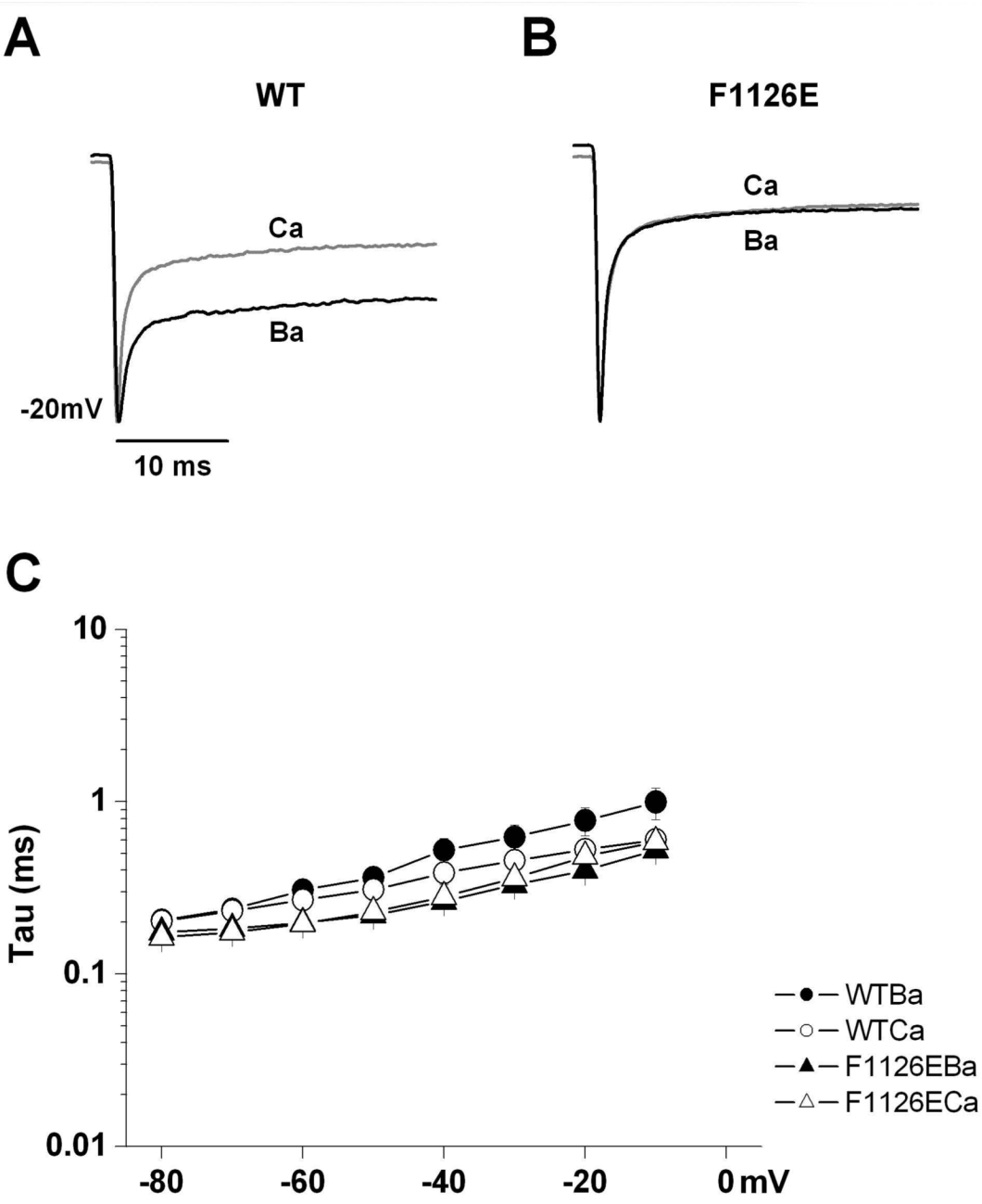

Fig. 6. F1126E does not affect deactivation time constants of the channel

Sample wild-type **(A)** and E1126E **(B)** tail currents were measured in 10 mM Ba^{2+} and 10 mM Ca^{2+} as indicated. Tail currents were elicited by repolarizing steps to −20 mV following 50 msec steps to +50 mV. Tail currents measured in Ca^{2+} were normalized to those measured in Ba^{2+} from the same cell. **(C)** To quantify deactivation time constants (τ) at the indicated voltages, raw data were fitted with a single exponential equation. Average τ at the indicated repolarization potentials are shown for wild-type (n = 8) and F1126E (n = 5) in Ba^{2+} and Ca^{2+}.

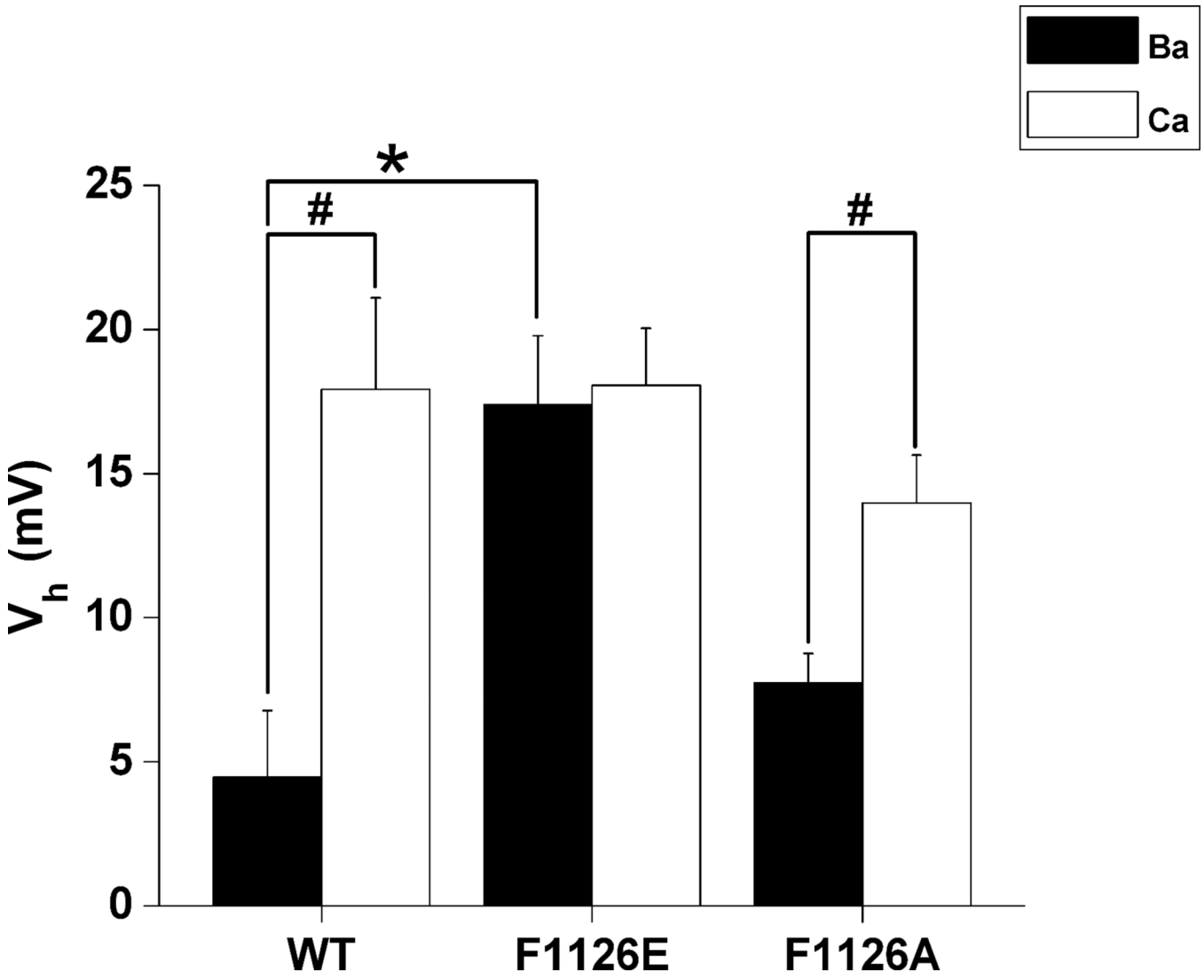

Fig. 7. Replacing Phe-1126 with alanine does not affect L-channel V_h

Half activation voltage (V_h) is plotted for wild-type, F1126E and F1126A channels with Ba^{2+} and Ca^{2+} as the ion carriers. F1126A (Ba^{2+}) V_h = 7.7 ± 1.0 mV, (Ca^{2+}) V_h = 14.0 ± 1.7 mV, n = 6. See Fig. 5 for more details.

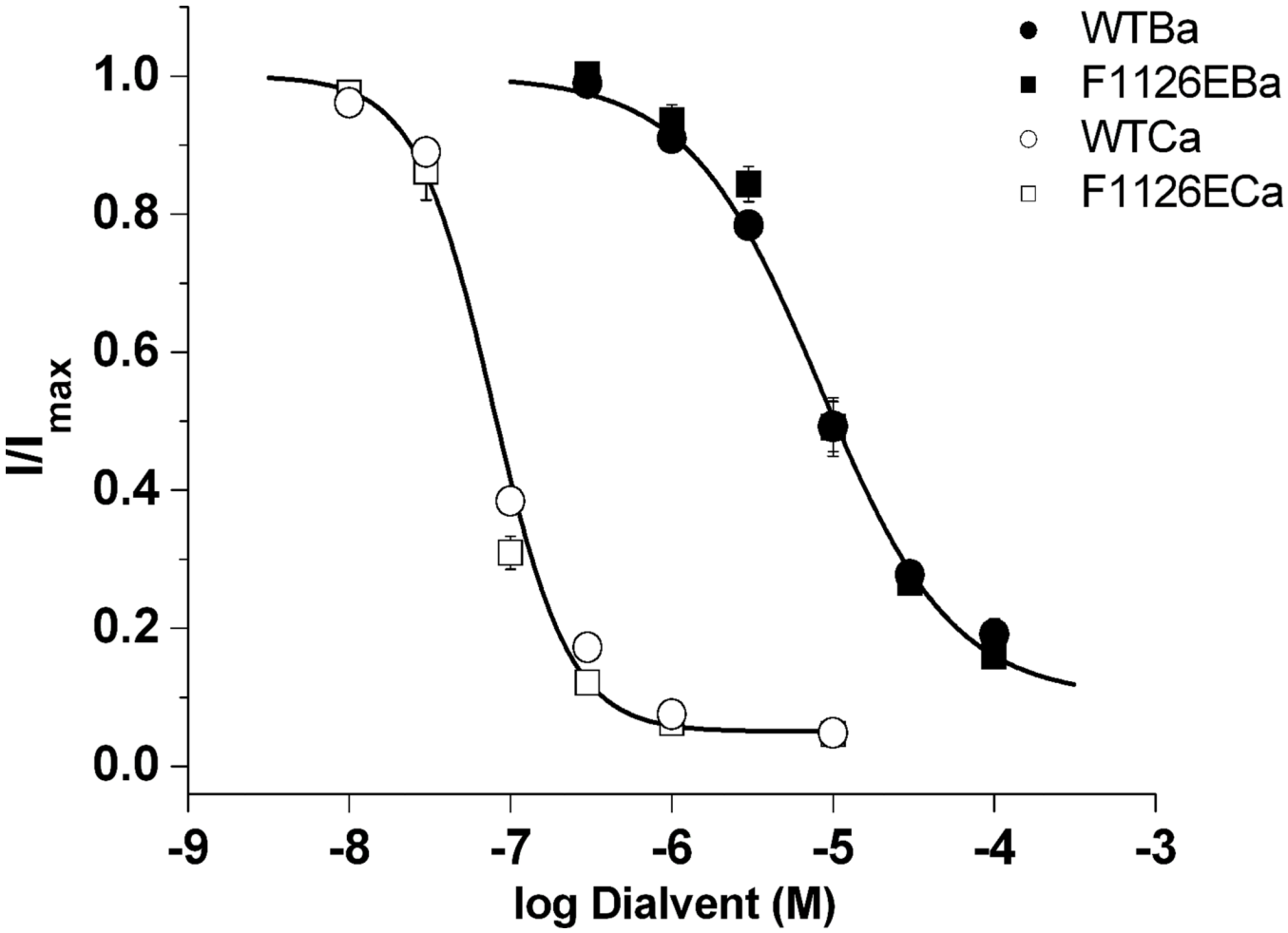

Fig. 8. High affinity binding of single Ba^{2+} and Ca^{2+} ions to the selectivity filter is not altered by the F1126E mutation

Tail-currents were evoked at −50 mV following 20 msec depolarizing steps to +30 mV to maximally activate wild-type and F1126E channels. Peak tail-currents measured at the indicated concentrations of free Ba^{2+} and Ca^{2+} were normalized to the maximum current amplitude determined from the Hill equation fit to the dose-response data from each cell. IC_{50} values determined in Ca^{2+} (nM): wild-type, 80.0 ± 3.7 (n = 6); F1126E, 67.0 ± 5.6 (n = 5); in Ba^{2+} (μM): wild-type, 9.3 ± 1.0 (n = 5); F1126E, 10.5 ± 1.2 (n = 6).

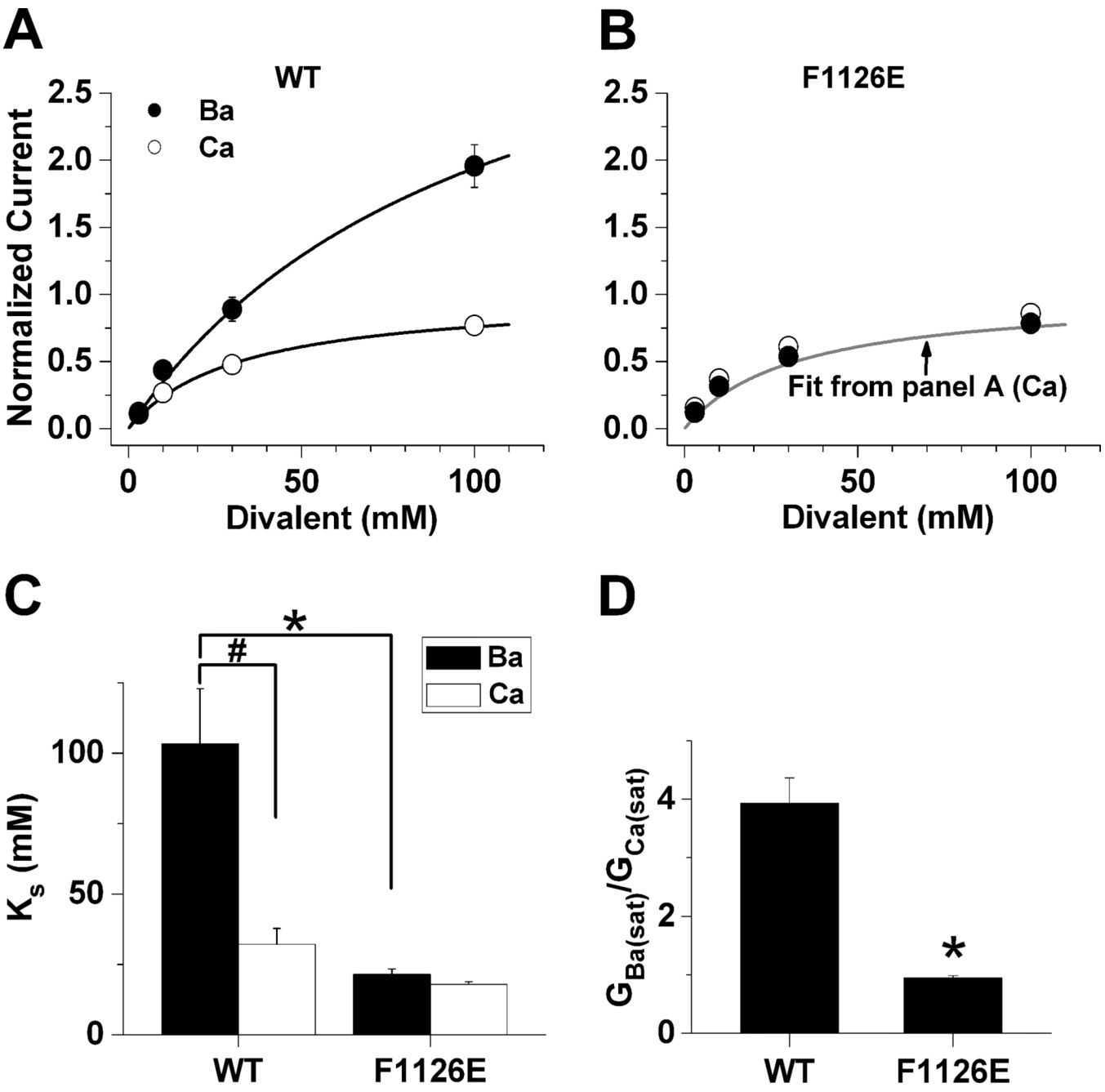

Fig. 9. F1126E alters the relationship between saturating and conductance of Ba^{2+}

Peak tail-currents were recorded at 0 mV following 20 msec depolarizing steps to +70 mV, to maximally activate wild-type (A) or F1126E (B) in Ba^{2+} and Ca^{2+}. Tail-currents were measured in 3, 10, 30 and 100 mM Ba^{2+} and Ca^{2+} from the same cell. Data were normalized to $G_{Ca(sat)}$ and fit by the Michaelis-Menton equation, $G = G_{sat}/(1 + (K_S/c))$, where G_{sat} is the level of current at saturating concentrations of divalent cations, c is the concentration of divalent cation, and K_S is the divalent cation concentration that produces one-half G_{sat}. The fit for wild-type (Ca^{2+}) is shown in panel B (gray). $G_{Ba(sat)}$ (nS), wild-type, 9.2 ± 2.9 (n = 5); F1126E, 3.6 ± 0.7 (n = 6); $G_{Ca(sat)}$: wild-type, 2.7 ± 1.3; F1126E, 3.7 ± 0.6. (C) K_S

values in mM are plotted for wild-type and F1126E in Ba^{2+} and Ca^{2+}. (D) Data are plotted as $G_{Ba(sat)}/G_{Ca(sat)}$ for wild-type and F1126E.